Quaternary Research 76 (2011) 253–263

Contents lists available at ScienceDirect

Quaternary Research

journal homepage: www.elsevier.com/locate/yqres

Late Quaternary paleoenvironments and paleoclimatic conditions in the distal Andean piedmont, southern Mendoza, Argentina

Alfonsina Tripaldi [a,*], Marcelo A. Zárate [b], George A. Brook [c], Guo-Qiang Li [d]

[a] Dept. of Geology, CONICET, Universidad de Buenos Aires, Ciudad Universitaria, Buenos Aires C1428EHA, Argentina
[b] INCITAP, CONICET, Universidad Nacional de La Pampa Avenida Uruguay 151, Santa Rosa, 6300 La Pampa, Argentina
[c] Department of Geography, University of Georgia, Athens, GA 30602, USA
[d] Center for Arid Environment and Paleoclimate Research (CAEP), MOE Key Laboratory of West China's Environmental System, Lanzhou University, 222 Tianshuinanlu, Lanzhou, Gansu, 730000, China

ARTICLE INFO

Article history:
Received 21 September 2010
Available online 31 July 2011

Keywords:
Ephemeral streams
Aeolian dunes
Luminescence ages
Last interglacial
Andean piedmont
Argentina

ABSTRACT

The Andean piedmont of Mendoza is a semiarid region covered by extensive and partially vegetated dune fields consisting of mostly inactive aeolian landforms of diverse size and morphology. This paper is focused on the San Rafael plain (SRP) environment, situated in the distal Andean piedmont of Mendoza (34° 30′S), and reports the sedimentology and OSL chronology of two representative exposures of late Quaternary deposits, including their paleoenvironmental and paleoclimatic significance. Eleven facies, including channel, floodplain, fluvio–aeolian interaction, and reworked pyroclastic and aeolian deposits, were described and grouped into two facies associations (FA1 and FA2). FA1 was formed by unconfined sheet flows, minor channelized streams and fluvial–aeolian interaction processes. FA2 was interpreted as aeolian dune and sand-sheet deposits. OSL chronology from the SRP sedimentary record indicates that between ca. 58–39 ka and ca. 36–24 ka (MIS 3), aggradation was governed by ephemeral fluvial processes (FA1) under generally semiarid conditions. During MIS 2, the last glacial maximum (ca. 24–12 ka), a major climatic shift to more arid conditions is documented by significant aeolian activity (FA2) that became the dominant sedimentation process north of the Diamante–Atuel fluvial system. The inferred paleoenvironmental conditions from the SRP sections are in broad agreement with regional evidence.

Introduction

During the past two decades, the loess–paleosol records of southern South America have received increasing attention as potential archives of Quaternary paleoclimates in order to understand more fully the conditions generated by climatic changes in the Southern Hemisphere. As a result several studies have reported the fossil content, geochronology and paleosol development of loess-paleosol sequences and alluvial successions of the eastern Pampas (Tonni et al., 1999; Prieto et al., 2004; Kemp et al., 2004, 2006; Frechen et al., 2009; Blasi et al., 2010), providing interpretations of past environmental and climatic conditions during the Quaternary.

Loess deposits are part of the largest mid-latitude aeolian system of South America, which covers the central and northern region of Argentina as well as areas of Uruguay, southern Brazil and Paraguay. The eastern Pampas loess grades into coarser textured deposits (sand dunes and sand mantles) across the western Pampas and the distal Andean piedmont (Fig. 1), a region scantily known despite being the source area for the late Quaternary aeolian system of central Argentina (Teruggi, 1957; Clapperton, 1993; Iriondo, 1999; Toms et al., 2004). A more detailed knowledge of this vast aeolian cover is significant for the understanding of the general aeolian dynamic of the system. Although recent studies have provided a better comprehension of the chronology and geomorphology of dune systems in some western areas of San Luis, La Rioja and San Juan provinces (Fig. 1) (Tripaldi and Forman, 2007), the distal Andean piedmont remains relatively unstudied. Only some paleoclimatic and paleoenvironmental studies have been performed based on pollen (D'Antoni, 1983; Markgraf, 1983) and mollusc assemblages (De Francesco et al., 2007) in piedmont settings of Mendoza. This area is covered by very extensive and partially vegetated dune fields, separated by permanent rivers flowing from the Andes Cordillera (Mendoza, Tunuyán, Diamante and Atuel) and minor ephemeral streams (Fig. 1). The dunes are mostly inactive aeolian landforms of diverse size and morphology, like transverse, longitudinal, parabolic and blowout dunes (González Díaz and Fauqué, 1993; Krömer, 1996; Perelló et al., 2009; Tripaldi, 2010).

Consequently, during the last three years further studies have been carried out at the San Rafael plain (SRP) situated in the Andean

* Corresponding author. Fax: +54 11 4576 3329.
E-mail addresses: alfo@gl.fcen.uba.ar (A. Tripaldi), mzarate@exactas.unlpam.edu.ar (M.A. Zárate), gabrook@uga.edu (G.A. Brook).

0033-5894/$ – see front matter © 2011 University of Washington. Published by Elsevier Inc. All rights reserved.
doi:10.1016/j.yqres.2011.06.008

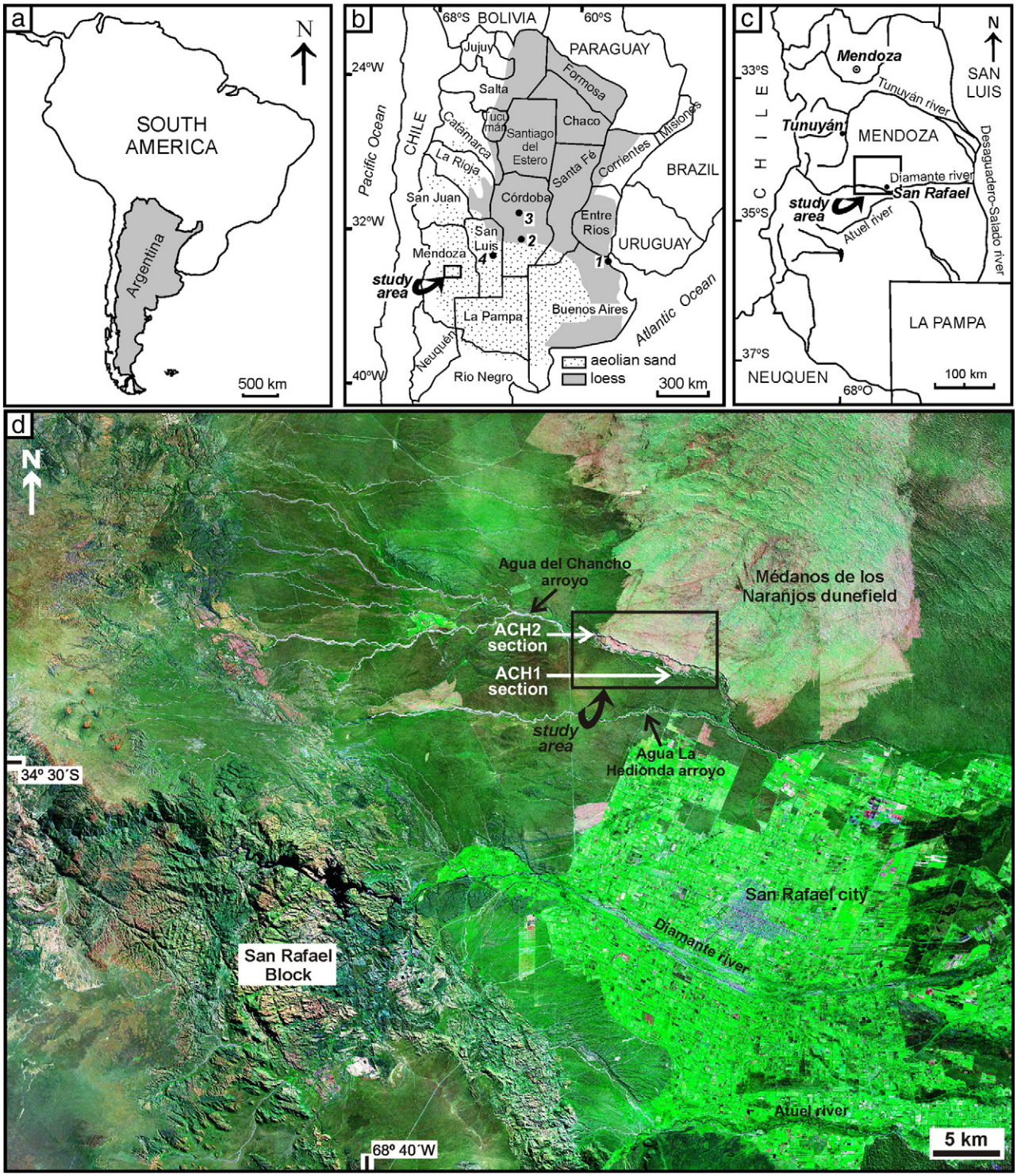

Figure 1. Location of study area: a and b, relation of the study sections to the aeolian sand (dotted) and loess (shaded) cover of Argentina, Paraguay, Brazil and Uruguay (modified from Zárate, 2003) and location of other aeolian localities mentioned in the text: 1, Baradero, 2, Río Cuarto, 3, Lozada, 4, San Luis dunefield; c, Mendoza province, boxed area is shown in d; d, Landsat ETM + image (https://zulu.ssc.nasa.gov/mrsid/) showing the study area and location of ACH1 and ACH2 sections in relation to the San Rafael block, the Diamante and Atuel alluvial plains and the Médanos de los Naranjos dunefield.

piedmont of central Mendoza (34°30′S) (Fig. 1c) with the aim of contributing to a better comprehension of the Quaternary paleoenvironmental and paleoclimatic evolution and the general dynamic of the aeolian system. The main objectives of this paper, as starting points, have been to analyze the nature and chronology of the Quaternary succession in the SRP. Therefore, the sedimentology of two late Quaternary exposures of the SRP (Fig. 1) is reported, providing the first OSL age estimates for the deposits in the region. The obtained results permitted to infer several intervals differentiated by the dominance of either fluvial or aeolian processes and correlate proximal and distal environments of the aeolian system of central Argentina.

https://doi.org/10.1016/j.yqres.2011.06.008 Published online by Cambridge University Press

Environmental and geological setting

The SRP is a semiarid environment with a mean annual precipitation of 350 mm and a mean annual temperature of 15°C (Prohaska, 1976). The region lies in the rain shadow of the Andes Cordillera, which reach 5000 to 6000 m elevation at this latitude. The great height of the Andes means that virtually no winter rain reaches the region from the Pacific. Instead, the climate is dominated by the Atlantic anticyclone with summer precipitation. Vegetation, part of the Monte phytogeographic province (Cabrera, 1971), is a shrub steppe of *Larrea* spp as well as Gramineae on dune systems (Rundel et al., 2007; Abraham et al., 2009).

The SRP is east of the San Rafael basement block, a range situated 40 km east of the Andes Cordillera front and composed of Middle Proterozoic metamorphic rocks as well as Paleozoic and Triassic sedimentary and volcanic units. The San Rafael block is part of an old peneplain uplifted during the Miocene–Pliocene by the Andean deformation (Ramos and Kay, 2006) (Fig. 1). Geomorphologically, the SRP is an extensive aggradational environment, made up of both fluvial and aeolian deposits exposed along riverbanks that form the southern end of a major plain, Depresión de la Travesía (Polanski, 1963; Rodríguez and Barton, 1993). It slopes from 900 m asl at the foot of the San Rafael block to 350 m asl in the east.

The SRP is crossed by two permanent rivers, Diamante and Atuel, with markedly seasonal discharge. These rivers, tributaries of the Desaguadero–Salado fluvial system, have excavated deep and narrow canyons across the uplifted San Rafael block (Fig. 1). During the last glaciation, the upper basins of both rivers were glaciated (Gosse, 1994; Espizúa, 2005). Thus, the Diamante and Atuel rivers discharged glacial meltwater and transported sediments from the Andes that accumulated downstream in the SRP. Dams along these rivers, constructed to meet the irrigation needs of the San Rafael agricultural region, have modified the original drainage system of the distal Andean piedmont. North of the fluvially dominated landscape of the Diamante and Atuel rivers, the SRP is dissected by other minor streams, mostly ephemeral, including Agua del Chancho and Agua La Hedionda arroyos that drain the eastern slope of the San Rafael Block (Fig. 1). The valleys of these two arroyos consist of a well-developed fill terrace and the present alluvial floodplain (Tripaldi et al., 2010).

The deposits of the SRP were grouped into two lithostratigraphic units, Villa Atuel at the base and Río Seco de La Hedionda at the top, considered to be Holocene in age based on regional correlations (González Díaz, 1972). More recently, the entire depositional sequence has been included in a single unit, the Villa Atuel Formation (Sepúlveda et al., 2007).

Methodology

This paper examines sedimentological facies in outcrops of the aggradational SRP exposed by channel incision along the riverbanks of Agua del Chancho arroyo. Two sections were examined ACH1 and ACH2 (Figs. 2, 3) and samples were taken for sediment analysis. Chronologies were developed for both sections using OSL dating. The geomorphology of the broader area was analyzed using aerial photographs and satellite imagery.

The ACH1 section is on the southern side of the Agua del Chancho arroyo (34°27.19′S, 68°23.47′W) and the upstream ACH2 section is on the northern side (34°25.67′S, 68°27.34′W, Fig. 1). Sedimentological studies followed the general approach to facies analysis proposed by Miall (1977, 1996). Lithofacies, reflecting depositional processes, were described and grouped into facies, as sub-environments, and the latter finally gathered in facies associations representing different sedimentary

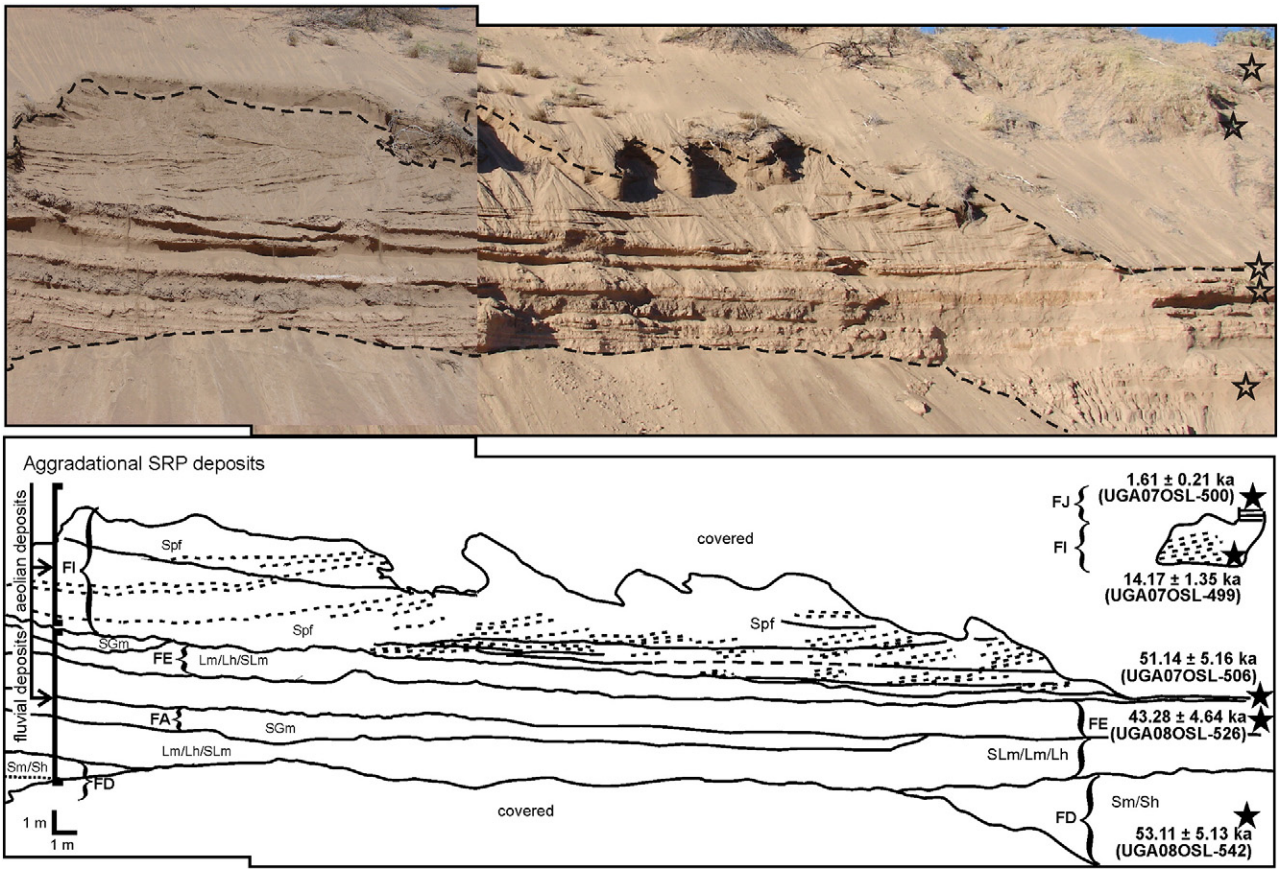

Figure 2. Facies tracing and field aspect of the SRP deposits at ACH1 section, facing N, showing the fluvial deposits of the lower part (Facies A, D, E), covered by cross-bedded aeolian sand (Facies I) and minor aeolian sand sheet on top (Facies J); stars indicate the position of OSL-dated samples and their corresponding ages.

https://doi.org/10.1016/j.yqres.2011.06.008 Published online by Cambridge University Press

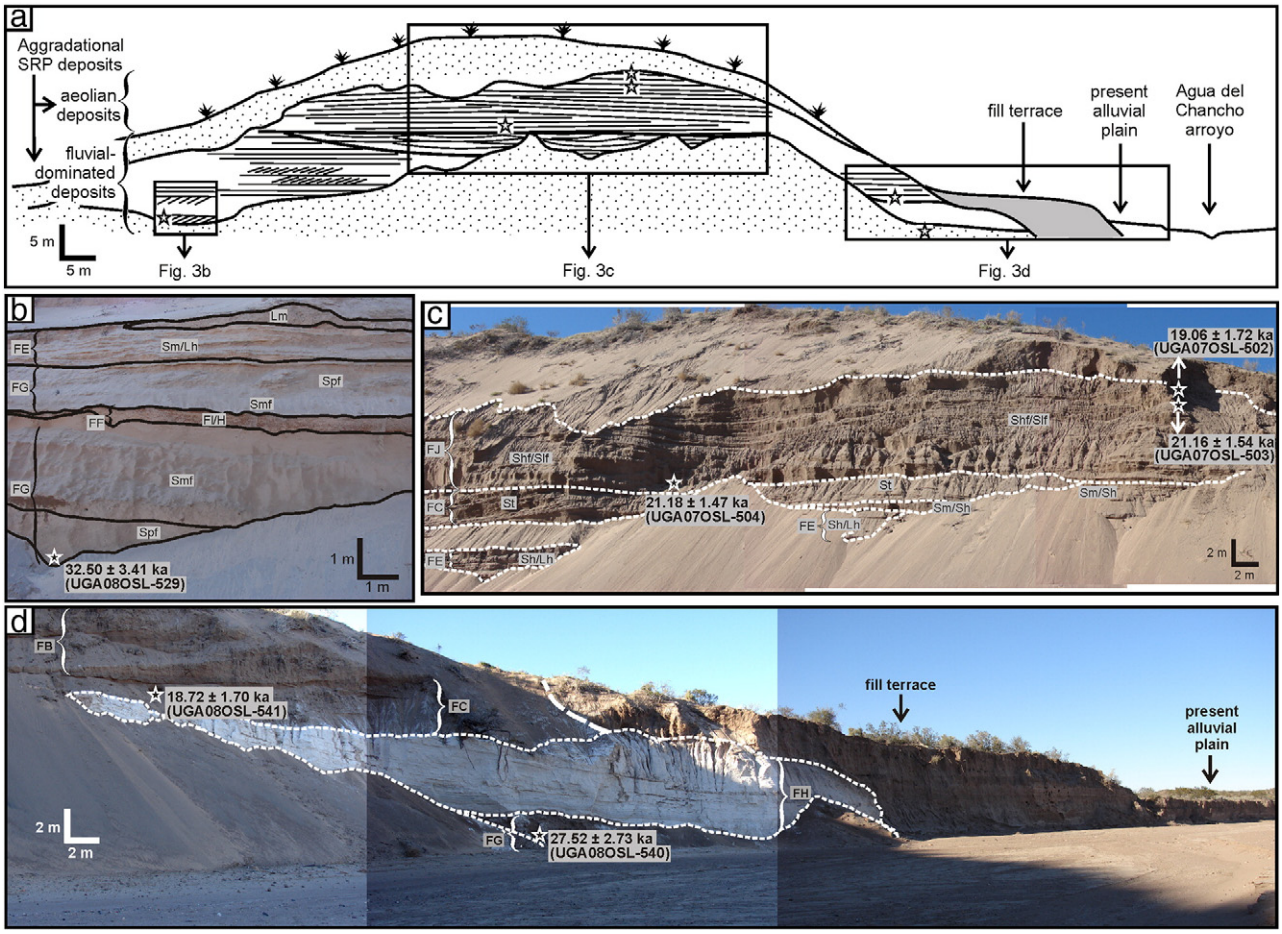

Figure 3. Facies tracing and field aspect of the SRP deposits at ACH2 section, facing S: a, general scheme of the ACH2 section with the location of the following pictures; b, fluvial–aeolian interaction (Facies G) and overbank (Facies E, F) deposits from the base of the section; c, overbank and bar deposits (Facies E, C) covered by aeolian sand sheet sand (Facies J) of the uppermost levels; d, reworked pyroclastic deposits (Facies H) interstratified with fluvial deposits (Facies B, C and G); stars indicate the position of OSL-dated samples and their corresponding ages.

environments (Tables 1 and 2). Lateral and vertical facies changes and assemblages were analyzed in facies logs (Figs. 2, 3). Representative bulk samples from the various facies in the studied sections were analyzed for grain-size distribution using a Malvern 2000 laser-based granulometer, at a quarter phi scale (Table 3). Statistical parameters were derived from the formulas and classifications of Folk and Ward (1957). Histograms and cumulative probability frequency curves were built and evaluated for each sample.

Samples for luminescence dating were collected only after completing a detailed stratigraphic analysis at the two sections, including definition of facies associations and their component facies and lithofacies. Samples were obtained above and below major

Table 1
Lithofacies identified in the aggradational SRP deposits at studied sections in the Agua del Chancho arroyo (modified from Miall, 1996).

Lithofacies	Description	Interpretation
Gmm	Massive, matrix-supported gravel	Cohesionless hyperconcentrated flows
SGm	Massive gravelly sand	Cohesionless hyperconcentrated flows
Gcm	Massive, clast-supported gravel	Channel lag or low longitudinal bars
Gch	Crude horizontally stratified, clast-supported (occasionally with high matrix content) gravel	Channel lag or low longitudinal bars
SGh	Crude horizontally stratified, clast-supported gravelly sand	Channel lag or low longitudinal bars
Sp	Planar cross-bedded, poorly sorted, very fine- to coarse-grained sand	2D megaripples
St	Trough cross-bedded, poorly sorted, medium- to coarse-grained sand	3D megaripples
Sh	Horizontally laminated, moderately to poorly sorted, very fine- to silty sand	Upper regime plane-bed flow
Sr	Ripple cross-laminated, medium- to fine-grained sand	Current ripples
Sm	Massive, very fine- to silty sand, in some beds sand is good sorted and presents scattered muddy rip up clasts, coarse-sand clasts and granules	Hyperconcentrated flows, normally from fluvially reworked aeolian sand
Lh/SLh	Horizontal laminated, occasionally diffuse, silt and sandy silt	Overbank suspension or very weak tractive currents
Lm/SLm	Massive silt and sandy silt	Overbank suspension or fine hyperconcentrated flows
Shf	Horizontal laminated, good to moderately sorted, fine to very fine-grained sand	Aeolian ripple migration
Slf	Very low angle cross-laminated, good to moderately sorted, fine to very fine-grained sand	Aeolian ripple migration
Smf	Good sorted, fine-grained to silty sand, massive or with diffuse lamination	Vertical accretion of a partially vegetated, aeolian mantle
Fl	Horizontal laminated mud	Overbank suspension
Tl	Tephra layer	Ashfall deposits

https://doi.org/10.1016/j.yqres.2011.06.008 Published online by Cambridge University Press

Table 2
Facies and facies associations in exposures of SRP deposits in the Agua del Chancho arroyo.

Facies	Lithofacies	Interpretation	Facies associations
A	Gcm, Gch, SGh SGm, Gmm	Channel lag or low longitudinal bar deposits Cohesionless hyperconcentrated flows	FA1
B	Sp, Sh	Low sandy transverse bars formed by 2D megaripples and upper regime plane-bed flow, planar bed flow deposits	
C	St	Sandy transverse bar formed by 3D megaripples	
D	Sh, Sm, Sr	Proximal overbank deposits	
E	Lm, Lh, SLh, SLm	Distal overbank deposits	Ephemeral, shallow and poorly confined creeks, with fluvial–aeolian interaction processes
F	Fl, H	Final waning stage floods or suspension fallout in small, temporary water bodies at the floodplain	
G	Spf, Shf, Sm, Fl, Tl	Fluvial–aeolian interaction deposits at the floodplain, formed by small aeolian dunes, aeolian ripples and fluvially reworked aeolian sand. Some intercalations of ashfalls	
H	Sm, Sh, Sr, Tl	Mostly reworked pyroclastic deposits with some intercalations of tephra layers	
I	Spf	Aeolian crescentic dunes	FA2
J	Shf, Slf, Smf	Aeolian sand sheet dominated by aeolian ripples and vertical accretion of a partially vegetated aeolian mantle	Dunes and aeolian sand sheet

stratigraphic boundaries by hammering an opaque plastic pipe horizontally into the vertical face of the exposure. Multiple samples (usually two or three) were collected from major fluvial or aeolian stratigraphic units to define the period of deposition. Thick layers of fine sand were preferred for sampling and great care was taken to avoid pedogenic horizons, areas showing possible bioturbation, and zones too close to stratigraphic boundaries where mixing of sediments of different origin and/or age might be possible. All sample locations were carefully marked on photo mosaics of the sediment sections. Representative samples of aeolian and fluvial sediments were collected to determine present moisture content as an aid in establishing long term moisture estimates for dose rate estimation.

In the laboratory, the potentially light-exposed portions at both ends of the sampling tubes were removed. All laboratory processes of sample preparation and luminescence measurement were carried out in subdued red light. All raw samples were treated with 10% HCl and 20% H_2O_2 to remove carbonate and organic matter. After drying, the samples were sieved to select the grain size in the size ranges of 90–125 μm, 125–180 μm and 180–250 μm. Heavy liquids of densities 2.62 and 2.75 g/cm^3 separated the grain fraction to obtain quartz and feldspar. The quartz grains were treated with 40% HF for 60 min to remove the outer layer irradiated by alpha particles and remaining feldspars. The grains were then treated with 1 mol/L HCl for 10 min to remove fluorides created during the HF etching. Pure quartz fractions with grains in the size range 125–180 μm were finally acquired.

The OSL measurements were carried out in the Luminescence Laboratory of the University of Georgia, using an automated RisøTL/OSL-DA-15 reader (Markey et al., 1997). Light stimulation of quartz mineral extracts was undertaken with an excitation unit containing blue light-emitting diodes ($\lambda = 470 \pm 30$ nm) (Bøtter-Jensen et al., 1999). Detection optics comprised two Hoya 2.5-mm-thick U340 filters and a 3-mm-thick stimulation Schott GG420 filter coupled to an EMI 9635 QA photomultiplier tube. Laboratory irradiation was carried out using 90Sr/90Y sources mounted within the reader, with dose rates of 0.0904 Gy/s.

The equivalent dose of quartz was determined by the SAR protocol (Murray and Wintle, 2000). The purity of quartz was checked by IRSL at 50°C and the result showed that none of the samples contained feldspar in the quartz fraction. The OSL dating recuperation test and dose recovery test showed that the SAR protocol was reliable for the samples examined in this study. Data were analyzed using the ANALYST program of Duller (1999).

Fluvial sediments may be insufficiently and/or unevenly bleached prior to burial. Whether fluvial samples were fully bleached prior to burial can be detected by examining the correlation between the De values and the sensitivity-corrected natural OSL signals (Zhang, et al., 2003). The six fluvial samples were analyzed in this way and only well-bleached aliquots were used to calculate the equivalent dose.

The environmental dose rate is created by the radioactive elements existing in grains of the sample and the surrounding sediments, with a small contribution from cosmic rays. For all the samples measured, a thick source Daybreak alpha counting system was used to estimate U and Th for dose rate calculation. K contents were measured by ICP90, using the sodium peroxide fusion technique at the SGS Laboratory in Toronto, Canada. All measurements were converted to alpha, beta and gamma dose rates according to the conversion factors of Aitken (1985). The dose rate from cosmic rays was calculated based on sample burial depth and the altitude of the section (Prescott and Hutton, 1994). Water

Table 3
Grain-size distribution of facies of the aggradational SRP deposits.

Sample	Facies	Mean	Sorting	Mode	Phi 1%	Median	Kurtosis	Skewness	%<62 μm
ACH0207-06	B	2.15	0.90	2.75–3.00 (0.00–0.25)	−0.19	2.25	0.88	−0.19	1.50
ACH0107-07	B	2.09	1.38	2.75–3.00 (−0.25/05)	−0.30	2.40	0.70	−0.30	6.00
ACH0107-01	D	2.49	1.06	3.00–3.25	−0.70	2.70	1.10	−0.30	3.90
ACH0107-02	D	2.65	0.85	1.50–1.75	1.30	2.50	0.80	0.20	7.80
ACH0107-04	D	2.81	0.93	3.00–3.25	0.50	2.70	1.00	0.00	9.60
ACH0207-01	G	2.15	0.61	2.00–2.25	0.87	2.19	1.00	−0.02	0.58
ACH0207-02	G	2.58	0.89	2.00–2.25	0.69	2.59	0.99	0.00	6.36
ACH0107-03	G	3.47	0.72	3.25–3.50	1.40	3.50	1.00	0.00	25.20
ACH0207-04	G	2.97	0.89	3.25–3.50	0.12	3.00	1.26	−0.11	12.22
ACH0207-05	G	2.52	0.83	2.75–3.00	0.17	2.48	1.00	−0.01	3.96
ACH0107-08	I	2.72	1.15	3.25–3.5 (−0.25/1.00)	−0.20	2.90	1.50	−0.30	10.8
ACH0107-09	I	2.59	0.94	3.00–3.25	0.30	2.50	1.00	0.00	5.70
ACH0207-07	J	2.66	0.74	2.75–3.00	0.27	2.72	1.23	−0.14	2.26
ACH0207-08	J	2.18	1.18	2.75–3.00 (0.00–0.25)	−0.29	2.44	0.94	−0.36	2.12
ACH0207-09	J	2.17	1.03	2.00–2.25	−0.14	2.27	1.04	−0.15	2.27
ACH0207-10	J	2.14	0.82	2.00–2.25	−0.33	2.20	1.11	−0.05	0.86

https://doi.org/10.1016/j.yqres.2011.06.008 Published online by Cambridge University Press

content of the fluvial sediment samples examined here must have changed drastically over time after they were buried. This is because conditions varied between more arid to less arid resulting in alternating periods of decreased and increased surface and groundwater flow. Therefore, estimation of the water content was based on what is known about the history of the deposits and on as-collected values of moisture content (which were all less than 5% of dry sample weight). Fluvial sands in the floor of the Agua del Chancho arroyo were also sampled and had moisture levels up to 11% of dry sample weight. Since it is not possible to accurately determine the mean water content during the sediment burial period, water contents of $5 \pm 2.5\%$ and $10 \pm 5\%$ were assumed in age calculations for aeolian and fluvial sediments, respectively. Fluvially reworked aeolian sand, and small aeolian dunes in a fluvial setting, were treated as fluvial sediments in assigning a water content. Radio-isotope concentrations used in dose rate calculation are listed in Table 4 along with paleodose and age estimates.

It is generally accepted that aeolian sands are well bleached during transport and so provide reliable ages for the time of deposition. However, some researchers question whether fluvial sediments are always fully bleached at the time they are deposited so that OSL ages for these sediments would be too old (see Aitken, 1998, p.153, Fig. 6.8). However, there is increasing evidence that many fluvial sediments are sufficiently well bleached during transport to make them suitable for OSL dating (e.g., Colls, et al., 2001; Stokes, et al., 2001; Wallinga, 2001). This appears to be the case in this study, because fluvial sediments at the ACH 2 site dated by OSL at ca. 36–17 ka are overlain by aeolian sediments (ca. 23–17 ka) that are of similar age to the youngest fluvial deposits. This suggests that if the aeolian sediments were bleached at the time of deposition then so were the fluvial deposits.

Results

Eleven facies, including channel, floodplain, fluvio–aeolian interaction, reworked pyroclastic and aeolian deposits, were identified and described in the aggradational SRP succession. These were grouped into two facies associations (Table 2).

Facies A is formed by clast-supported, medium-grained to gravelly sand and fine gravel, that appear in thin (10–50 cm thick) tabular massive beds or with crude horizontal stratification (lithofacies Gcm, Gch, SGh). A few layers of massive and matrix-supported fine gravel and gravelly sand occur locally (lithofacies Gmm, SGm), passing into clast-supported gravel (Gcm). Facies A is the dominant channel unit in the SRP aggradational environment (Fig. 2). It is interpreted as the product of channel lag or low-relief sheet deposition below high energy gravel and gravelly sand transport (Hein and Walker, 1977). Occasionally, fine-grained gravity flows are also suggested by the occurrence of matrix-supported gravel and massive coarse-grained sand (Miall, 1996). The dominance of tabular beds, their extensive lateral continuity, traced for tens of meters, and absence of channel geometries (Fig. 2) suggest Facies A was formed by sheet-flood events, possibly by aggradation of very low longitudinal bars or lag deposits.

Facies B consists of horizontally and cross-bedded stratified sand forming thin (10–30 cm thick), tabular to lentiform bodies. It is made up of poorly to moderately sorted very fine- to coarse-grained sand (Table 3), showing horizontal laminations and planar cross-bedding (lithofacies Sh, Sp, Fig. 3). Facies B indicates channel deposits, reflecting low transverse bars as suggested by the occurrence of thin cross-bedding, formed by migration of 2D megaripples, and, in some cases, horizontally laminated levels at the top due to upper flow regime deposition (Williams, 1971; Miall, 1996).

Facies C was found only in ACH2 section. It comprises a lenticular body of irregular base made up of trough cross-bedded, medium- to coarse-grained sand (lithofacies St, Figs. 3a, c). Individual sets show variable thickness between 20 and 60 cm that can be traced laterally for up to 15 m. The thicker and more laterally extensive trough cross-bedding of Facies C suggests sedimentation by 3D megaripples, under lower flow regime conditions, likely forming transverse bars (Williams, 1971; Miall, 1996). The lenticular and irregular-based body of the deposits is interpreted as a partially confined channel filling.

Facies D includes moderately sorted, medium- to fine-grained sand (Table 3), sometimes with very thin and discontinuous mud drapes. These deposits occur mainly as centimeter thick, tabular beds, laterally traceable for tens of meters (Fig. 2). Locally, a lenticular, up to 2 m thick and irregular-based body of Facies D occurs at ACH1 (Fig. 2). Structureless beds and faint horizontal laminations are dominant; ripple lamination or beds with better preserved horizontal laminae are occasionally present (lithofacies Sm, Sh, Sr). Carbonate rhizoconcretions are common (Fig. 4a) as well as muddy rip-up clasts of variable size (coarse-grained sand through 10-cm pebbles) and shape (rounded to irregular) that are sometimes roughly aligned.

Facies D is interpreted as overbank deposition during extraordinary flood events. The dominance of massive and faintly laminated beds suggests rapid sedimentation from highly concentrated flows (Newell, 2001; Svendsen et al., 2003), possibly as sandy-silty gravity flows. Besides, the textural characteristics of Facies D beds with absence of gravel-sized clasts, a fine sand mean grain size, moderate sorting and symmetrical or slightly positive skewness, point to a

Table 4
OSL dosimetry and age data for samples of the aggradational SRP deposits at ACH1 and ACH2 sections.

Laboratory number	Sample ID	Fluvial (F) or aeolian (A)	Number of aliquots[a]	D_e (Gy)	U (ppm)	Th (ppm)	K (%)	Water content (%)	Cosmic dose rate (Gy/ka)[b]	Dose rate (Gy/ka)	Age (ka)
ACH1 section											
UGA08OSL-542	CHAN-1	F	14	170.56 ± 7.92	3.23 ± 0.47	6.93 ± 1.61	2.14 ± 0.1	10 ± 5	0.15	3.42 ± 0.22	53.11 ± 5.13
UGA08OSL-526	CHAN-2	F	6	141.06 ± 6.55	3.49 ± 0.68	6.87 ± 2.34	2.09 ± 0.1	10 ± 5	0.19	3.46 ± 0.28	43.28 ± 4.64
UGA07OSL-506	CHAN-3	F	12	167.94 ± 8.49	3.73 ± 0.55	6.03 ± 1.9	2.09 ± 0.1	10 ± 5	0.22	3.43 ± 0.23	51.14 ± 5.16
UGA07OSL-499	CHAN-4	A	14	42.78 ± 2.72	2.81 ± 0.5	6.42 ± 1.7	1.87 ± 0.1	5 ± 2.5	0.19	3.02 ± 0.21	14.17 ± 1.35
UGA07OSL-500	CHAN-5	A	12	4.65 ± 0.54	2.92 ± 0.41	5.76 ± 1.43	1.73 ± 0.1	5 ± 2.5	0.22	2.90 ± 0.19	1.61 ± 0.21
ACH2 section											
UGA08OSL-529	ELCH-1	F	9	123.35 ± 5.91	4.65 ± 0.75	5.27 ± 2.56	2.56 ± 0.1	10 ± 5	0.17	3.98 ± 0.30	32.50 ± 3.41
UGA08OSL-540	ELCH-2	F	9	90.73 ± 4.66	3.21 ± 0.53	6.47 ± 1.81	2.3 ± 0.1	10 ± 5	0.18	3.30 ± 0.28	27.52 ± 2.73
UGA08OSL-541	ELCH-3	F	15	62.83 ± 2.59	3.73 ± 0.48	6.31 ± 1.65	2.21 ± 0.1	10 ± 5	0.22	3.36 ± 0.27	18.72 ± 1.70
UGA07OSL-504	ELCH-4	A	17	72.03 ± 2.36	3.47 ± 0.44	7.49 ± 1.54	2.04 ± 0.1	5 ± 2.5	0.19	3.40 ± 0.21	21.18 ± 1.47
UGA07OSL-503	ELCH-5	A	15	61.63 ± 2.48	2.61 ± 0.35	5.79 ± 1.22	1.82 ± 0.1	5 ± 2.5	0.22	2.91 ± 0.18	21.16 ± 1.54
UGA07OSL-502	ELCH-6	A	12	58.35 ± 2.69	3.04 ± 0.59	5.6 ± 2.03	1.89 ± 0.1	5 ± 2.5	0.22	3.06 ± 0.24	19.06 ± 1.72

[a] Grain size was 125–180 μm.
[b] The error for the cosmic ray dose rate is estimated as ±0.02 Gy/ka in the dose rate calculation.

https://doi.org/10.1016/j.yqres.2011.06.008 Published online by Cambridge University Press

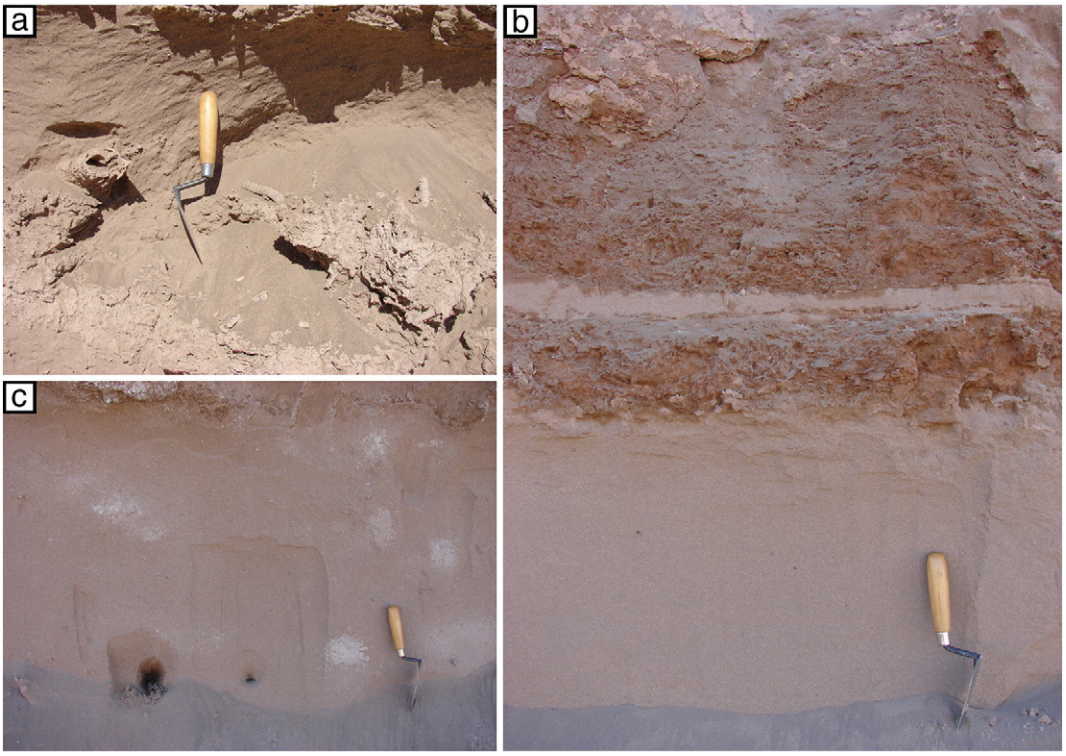

Figure 4. Field aspect of some levels of the SRP deposits. a, heterolithic beds (Facies F) covering a massive fine sand bed (Facies G) at ACH2 section; b, carbonate rhizoconcretions in overbank facies at ACH1 section; c, intense animal burrowing in a sandy bed underlying a tephra layer at ACH2 section.

primary aeolian origin of the sediments, later reworked by current processes (fluvially reworked aeolian sand of Newell, 2001).

In other beds, the occurrence of horizontal lamination indicates deposition under upper flow regime plane-bed conditions, while those deposits with rippled lamination point to sedimentation under weak traction currents during waning stage of flood events (Williams, 1971). Facies D, especially when occurring in lenticular beds, would represent infilling of abandoned or secondary channels, while the dominant tabular bodies suggest sedimentation by unconfined sheet flows (Hampton and Horton, 2007). The presence of carbonate rhizoconcretions denotes seasonal conditions as well as an exposed and vegetated floodplain area (possibly with weak paleosol development).

Facies E is similar and closely associated to Facies D but it is characterized by sandy silt and silt in massive or horizontally laminated tabular beds (lithofacies SLm, SLh, Lm, Lh; Table 1), with much more common and thicker mud drapes. This facies may be traced laterally for tens of meters (Figs. 2, 3). Most of the beds have planar lower contacts while some others show more irregular surfaces. The occurrence of rhizoconcretions and muddy rip-up clasts is also very common. At ACH1 section, a fluvial sand sample from the base of the succession yielded an age of 53.11 ± 5.13 ka (58–48 ka) (UGA08OSL-542), while two sand samples from the topmost fluvial beds provided ages of 43.28 ± 4.64 ka (48–39 ka) (UGA08OSL-526) and 51.14 ± 5.16 ka (56–46 ka) (UGA07OSL-506) in a lower and upper bed, respectively (Fig. 2, Table 4). These ages suggest a period of fluvial deposition at this locality between ca. 58–39 ka.

Facies E is interpreted as overbank flood deposits from weak currents during the final stages of flooding and, according to their finer grain size, in a likely more distal location to the main channel than Facies D sediments (Guccione, 1993; Bridge, 2003). As in Facies D, rhizoconcretions indicate seasonal conditions on a vegetated floodplain.

Facies F consists of thin (up to 30 cm thick) lenticular mud layers, of very rare occurrence among the SRP deposits (Fig. 4b). It is made up of red to pale brown silty clay either in horizontally laminated or finely interlayered beds, with very fine-grained to silty sand in heterolithic structures (lithofacies Fl, H). Mottling, ferruginous nodules and frequent oxidized root traces are present. These features suggest that Facies F accumulated by clay suspension fallout in temporary small water bodies situated in the floodplain, accompanied by sporadic fine sand deposition due to very weak currents (Miall, 1996). Ferruginous nodules and oxidized root traces in Facies F reveal a vegetated floodplain area and oxidizing conditions.

Facies G is composed of moderately sorted to moderately well sorted, symmetrical, medium- to fine-grained sand occurring in massive, horizontally laminated or planar cross-bedded sets (lithofacies Sm, Sh, Spf; Figs. 3a, b; Tables 1 and 3). Massive sandy or sandy-silt layers, forming tabular beds up to 20 cm thick, are very common in Facies G. Occasionally, these beds contain scattered muddy rip-up clasts and carbonate concretions. Very thin and horizontally laminated sand is interstratified with the massive beds. Sandy cross-beds are arranged in tabular sets, with thickness varying from 0.80 m to 1.20 m. In some cases, foreset beds of adjoining sets show opposite paleocurrents. A cross-bedded sand of Facies G at the base of ACH2 section provided an age of 32.50 ± 3.41 ka (36–29 ka) (UGA08OSL-529) (Table 4, Figs. 3a, b).

An aeolian origin is attributed to these deposits on the basis of the lithological homogeneity, mean grain size in fine and very fine sand, moderate to moderately well sorting, low silt–clay content, and symmetrical-unimodal granulometric distributions of some representative levels of Facies G (ACH0207-02 and ACH0207-05 in Table 3), together with the presence of fine horizontal lamination and cross-bedding and absence of gravel sediments. Horizontally laminated sandy translatent strata (lithofacies Shf) were formed by migration of wind ripples (Hunter, 1977a), while thin cross-bedded sandy layers (Spf) indicate the development of small crescentic dunes (Hunter, 1977b).

Other levels of Facies G are formed by massive sand and silty sand beds with few isolated muddy rip-up clasts and carbonate concretions; some of them show moderate to moderately well sorted, symmetrical-unimodal granulometric distributions (e.g., ACH0207-01, ACH0207-03

https://doi.org/10.1016/j.yqres.2011.06.008 Published online by Cambridge University Press

and ACH0207-04 in Table 3), these levels are interpreted as fluvially reworked aeolian sand (Newell, 2001). The absence of structures suggests rapid sedimentation from flows with high concentration of sediment, likely related to the abundance of sand in floodplain areas due to aeolian accumulation (Langford, 1989).

Facies G is closely interstratified with overbank silty sand, sandy silt, and mud of Facies D, E and F, implying that mixed aeolian–fluvial deposits occurred more commonly on the floodplains, where, in addition, they have a higher probability of preservation in relation to channel area.

Facies H is composed of pyroclastic deposits including several tephra layers of variable thickness (3 cm to 2 m). Two massive tephra layers, one of them overlying a massive sandy bed with evidence of extensive animal burrowing (Fig. 4c), are interstratified with the fluvial–aeolian and floodplain deposits at the lower part of ACH2 section. A thin (less than 10 cm), white and massive tephra layer occurring a few centimeters below the present depositional surface is found at both sections and all along the riverbanks of Agua del Chancho arroyo. The later one is related to the 1932 eruption of the Quizapú volcano, situated towards the SW of the study area, that covered extensive areas of central Argentina with volcanic ash (Hildreth and Drake, 1992). These three pyroclastic levels are interpreted as primary tephra layers.

At ACH2 there is also a conspicuous, up to 2-m-thick, white pyroclastic-sedimentary body (Facies H), interstratified with fluvial deposits (Fig. 3d) and resting on a very irregular surface. It is dominantly composed of fine- to coarse-grained sand-size particles and shows mostly parallel stratification. Beds roughly follow the undulating lower contact, while horizontal laminations occur at the top of the deposit. Horizontal laminations alternate with medium to massive (up to 25 cm) beds, while thin ripple laminations are less common. On the basis of its lithological characteristics most of this body is interpreted as a mostly mixed pyroclastic-sedimentary deposit produced by the fluvial reworking of pyroclastic sediments (Cas and Wright, 1987). However, a primary volcanic ash fall origin cannot be ruled out for some white, rather massive layers included in the deposit. OSL ages for underlying and overlying fluvial beds gave bracketing ages of 27.52 ± 2.73 ka (30–25 ka) (UGA08OSL-540) and 18.72 ± 1.70 ka (20–17 ka) (UGA08OSL-541) for this deposit (Table 4, Fig. 3d).

The upper part of the regional aggradational SRP is entirely formed by fine sand, with planar, high-angle cross-laminations (lithofacies Spf, Facies I) and massive or horizontal to very low-angle cross-laminations (lithofacies Sm, Shf, Slf, Facies J; Table 1). In both facies, the mean grain size is fined sand, with unimodal and moderately sorted distributions and less than 6% silt-clay content (Table 3). Other samples have a main mode in fine sand but more abundant coarse and medium sand yielding incipient bimodal distributions (Table 3).

The upper part of the ACH1 section consists mostly of Facies I, reaching up to 7 m in thickness. It is in turn covered by 4 m of Facies J (Fig. 2). Cross-bedding units in Facies I are 2 to 3.5 m thick, with foreset beds dipping to the E–SE. A sample of cross-bedded sand from this section yielded an age of 14.17 ± 1.35 ka (16–13 ka) (UGA07OSL-499), while a sample from a faintly laminated horizontal bed of sand in Facies J dated to 1.61 ± 0.21 ka (1.8–1.4 ka) (UGA07OSL-500) (Table 4, Fig. 2).

Facies J comprises the upper 15 m of ACH2 section and exhibits parallel and very low-angle cross-laminated beds interlayered with deposits dominated by fine- and coarse-grained sand (Figs. 3a, c). Foreset beds in the low-angle cross-bedded units dip northwards. Some massive or faintly laminated horizontal sand layers also appear in this facies, mainly in the upper part. Gypsum rosettes up to 3 cm in diameter occur throughout Facies J. An age of 21.18 ± 1.47 ka (23–20 ka) (UGA07OSL-504) was obtained from the basal sand of this facies and ages of 21.16 ± 1.54 ka (23–20 ka) (UGA07OSL-503) and 19.06 ± 1.72 ka (21–17 ka) (UGA07OSL-502) were obtained from the topmost laminated and undisturbed deposit and the lower bed (Table 4, Fig. 3d). These ages suggest rapid deposition of Facies J in ACH2 in the interval ca. 23–17 ka.

Facies I and J are interpreted as aeolian deposits because of the dominance of fine-grained sand, absence of gravel and presence of very fine horizontal or cross-laminations. The cross-bedded sand of Facies I were formed by crescentic dune migration (Hunter, 1977b). Facies J was generated by wind ripple accumulation (Hunter, 1977a), in a sand sheet setting as suggested by the absence of interstratified cross-bedding, very low angle cross-laminations and textural features like bimodality and moderate to poor sorting (Fryberger et al., 1979; Kocurek and Nielson, 1986). The non-uniform textural patterns of the aeolian facies described could be also related to the considerable interaction with current processes.

Paleoenvironmental interpretation

The SRP deposits were grouped into two facies associations (Table 2). Facies Association 1 (FA1) appears to be largely of fluvial origin, being composed of sediments formed by sub-aqueous current processes, as well as by fluvial–aeolian interaction. Facies Association 2 (FA2), comprising Facies I and J, is interpreted as aeolian deposits. FA1 clearly forms the lower part of the SRP succession while FA2 appears in the upper part, in both ACH1 and ACH2 sections. This pattern of fluvial facies below and aeolian sand on top was observed not only in the two detailed surveyed and sampled sections, about 10 km apart, but also in several other exposures along the Agua del Chancho arroyo (boxed area in Fig. 1d).

FA1 is characterized by thin and laterally extensive tabular beds, mainly composed of overbank deposits interstratified with some channel and fluvially reworked aeolian units (Table 2). The channel units are mostly composed of channel lag and low longitudinal bar deposits, with some transverse bar deposits and, rarely, gravity flow beds (Fig. 2). The dominance of thin tabular beds of massive and horizontally stratified gravelly sand and fine gravel in the channel facies suggests sedimentation by unconfined sheet flows (Hampton and Horton, 2007). The described features indicate shallow and poorly confined channels with a gravel–sand substrate. The presence of transverse bar deposits, in some cases in lenticular units (facies B and C), implies there was also some fluvial deposition by bedform migration in deeper channels. Williams (1971) noted that 2D and 3D bedforms are common today in sandy ephemeral streams after very large floods. Similar deposits were also described by McKee et al. (1967).

The channel facies are accompanied by widespread tabular beds of laminated sand, silty sand and silts deposited by overbank sheet floods. Bull (1997) pointed out that modern discontinuous semiarid streams show significant fluvial aggradation governed by mantle overbank floods which accumulate thick, mostly massive, silty-sandy beds, very similar to the studied deposits. Sandy beds are common features in arid and semiarid rivers, as they are deposited in the floodplain by vertical accretion associated with the coalescence of islands and the infilling of abandoned channels (Nanson and Croke, 1992).

These sedimentological features portray a fluvial paleoenvironment consisting of a poorly integrated network of ephemeral, shallow and poorly confined creeks, with unconfined floodplains. This fluvial setting is comparable with the facies model of terminal fluvial systems proposed by Cain and Mountney (2009). In such a model, and according to the features of the SRP facies, these deposits would hypothetically correspond to a distal region of terminal fluvial systems characterized by sheetflood and overbank sedimentation, scarce channelized flows and a significant aeolian component represented by dunes, ripple accretion and massive sand (sand sheet).

Ephemeral streams in semiarid settings are typically associated with aeolian processes, so that fluvial–aeolian interaction deposits are common (Glennie, 1970; Langford, 1989; Bullard and Livingstone, 2002; Tripaldi and Limarino, 2008). The episodic nature of ephemeral stream flows, together with the scarce vegetation cover of semiarid environments, causes the exposed loose sand to be reworked easily by wind. Diverse fluvial–aeolian processes may take place giving way to the

https://doi.org/10.1016/j.yqres.2011.06.008 Published online by Cambridge University Press

formation of various bedforms and deposits in ephemeral stream plains (Langford, 1989). The massive fine sand and silty sand of the ACH1 and ACH2 sections is interpreted as fluvially reworked aeolian sand due to hyperconcentrated flows (Newell, 2001). In ephemeral stream environments the availability of sand, when accompanied by winds strong enough to transport it, allows the development of aeolian bedforms, as the here-recognized dune and ripple migration deposits. Later, these bedforms can be partially or entirely reworked by fluvial currents. In these fluvial settings, the abundance of sand and silt also promotes the development of hyperconcentrated flow deposits, a characteristic feature of ephemeral stream facies (Tripaldi and Limarino, 2008). These have been observed in the SRP sediment sections (Fig. 3b). The presence of fluvial–aeolian interaction deposits in the SRP is not surprising given that the studied sections are at the southern margin of the Médanos de los Naranjos dune field (Fig. 1d).

This aeolian system would have supplied large amounts of sand to the streams but it is clear that fluvial processes dominated aeolian processes during deposition of the basal sediments at both ACH 1 and ACH 2 sections. Aeolian deposits are not very common in these fluvial-dominated sediments, as indicated by infrequent wind ripple and dune beds in the sequences.

The aeolian deposits of FA2 overlie the ephemeral fluvial units of FA1. At ACH1 section, FA2 is dominated by cross-bedded fine sand deposited during the migration of crescentic dunes. Bed thickness varies from 2 to 3.5 m, possibly representing small-scale dunes or larger bedforms since the internal structure of crescentic dunes is sometimes very complex, including many sets of variable thickness (Ahlbrandt and Fryberger, 1982; Pye and Tsoar, 1990). The dip of foreset beds shows that depositing paleowinds were from the W–NW. In the uppermost 4 m of the ACH1 section, the presence of faintly laminated, horizontally bedded sand suggests vertical accretion of a partially vegetated aeolian sand sheet.

In ACH2 section, the prevalence of horizontal and very low-angle cross-laminations suggests that sedimentation was dominated by aeolian ripple migration (Hunter, 1977a). Moreover, as intercalations of cross-bedding were not identified, these deposits indicate an aeolian sand-sheet environment (Fryberger et al., 1979). The frequent occurrence of gypsum rosettes may indicate fluctuating groundwater levels during deposition.

Paleoclimatic implications

The sediments at ACH1 and ACH2 sections were deposited during the last ca. 58 ka and are a record of changing climate/hydrology in the SRP area. They delimit at least five climate/hydrologic intervals (labeled 1–5 in Fig. 5) that can be compared with the Greenland GISP 2 oxygen isotope record and Marine Isotope Stages (MIS; Martinson et al., 1987). Periods 1–3 occurred during MIS 3 while periods 4 and 5 are broadly equivalent to MIS 2 and 1, respectively. Period 1 lasted from ca. 58–39 ka and is defined by the basal fluvial beds (FA1) at ACH1. These beds suggest a fluvial system dominated by sheetflood processes in an ephemeral setting. The OSL chronology indicates that fluvial aggradation occurred between ca. 58 ka and 39 ka, according to the ages for UGA08OSL-542, UGA08OSL-526 and UGA07OSL-506 samples. In ephemeral streams, which at times can be almost dry and at other times can produce rare large floods, sedimentation takes place mainly during the flood events so that these dominate the sedimentary record. Aeolian activity may have been relatively insignificant during Period 1, which corresponds to the most prolonged warm interval during MIS 3, which lasted from ca. 59–24 ka. This correspondence suggests that slightly warmer conditions globally were conducive to increased fluvial activity in the SRP area (Fig. 5).

The fluvial-dominated setting of Period 1 was followed by an interval of stability and soil formation during Period 2, which lasted from ca. 39–36 ka (Fig. 5). Root casts and oxidation features at the top of FA1 in the ACH1 section record this interval and indicate a period of moist conditions. Furthermore, the absence of fluvial and aeolian sediments at ACH1 and ACH2 during Period 2 suggests a combination of reduced fluvial activity (reduced sediment supply for aeolian reworking) and migration of stream channels away from the area.

Fluvial deposits at ACH2 section indicate that streams were again active in the SRP area from ca. 36–24 ka (Period 3 in Fig. 5). However, the lack of fluvial sediments of these ages at ACH1 section shows that none of the channels were close to this location. The presence of more mixed fluvial–aeolian facies in ACH2 section reveals that aeolian processes were more active during Period 3 than during Period 1. The ACH2 section also contains reworked pyroclastic facies from a volcanic event that supplied material to the fluvial system. Bracketing OSL ages on underlying and overlying fluvial sands indicate that the volcanic eruption occurred sometime between ca. 30 ka and 17 ka. It is possible that these ages (UGA08OSL-540 and UGA08OSL-541 samples, Table 4) record different fluvial episodes separated by a more arid interval during which the volcanic ash accumulated before being buried by later fluvial deposits (Fig. 3).

Aeolian sedimentation (FA2) dominated Period 4 (24–13 ka) beginning ca. 23–20 ka at ACH2 (23–20 ka, UGA07OSL-504; 23–20 ka, UGA07OSL-503; 21–17 ka, UGA07OSL-502; Table 4, Fig. 5), and possibly

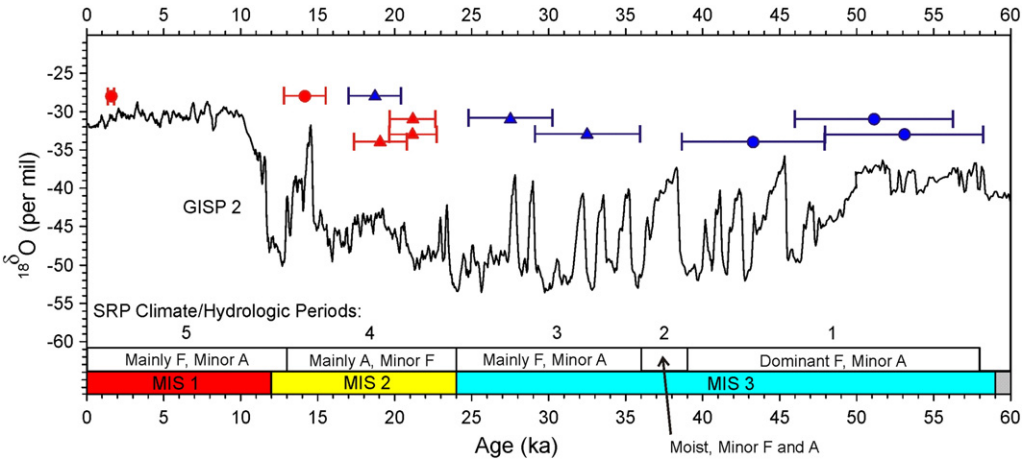

Figure 5. Periods of fluvial and aeolian activity in the SRP compared with the Greenland GISP 2 oxygen isotope record and Marine Isotope Stages (MIS; Martinson et al., 1987). Proposed SRP climate/hydrologic periods 1–5 are shown where F = fluvial and A = aeolian. Sediment ages are shown with error bars. ACH1 ages shown by circles and ACH2 ages by triangles. Red symbols denote aeolian sediments and blue symbols fluvial sediments.

https://doi.org/10.1016/j.yqres.2011.06.008 Published online by Cambridge University Press

continuing until ca. 16–13 ka based on the age for UGA07OSL-499 (14.17 ± 1.35 ka) from the ACH1 section (Table 4, Fig. 2). However, there was clearly some fluvial activity during Period 4 given the youngest age for fluvial deposits at ACH2 of 18.72 ± 1.70 ka (UGA08OSL-541, Table 4). The fluvial activity probably supplied sediment that was later transported by wind. Given higher $\delta^{18}O$ values in the GISP 2 core during MIS 2 than during the later stages of MIS 3 (Fig. 5; Martinson et al., 1987), it is possible that increased aeolian activity across the SRP was linked to higher wind velocities triggered by steeper global pressure gradients during the last glacial maximum, rather than simply drier conditions.

After ca. 13 ka, during Period 5 and broadly equivalent to MIS 1 (Fig. 5; Martinson et al., 1987), there was stream incision at ACH1 and ACH2 as the present channel established itself. Previously deposited aeolian and underlying fluvial sediments were cut and exposed in section along the river valley. The events of Period 5 may have been triggered by the warming that accompanied the beginning of MIS 1, the early Holocene (Fig. 5). However, as indicated by an OSL age of 1.61 ± 0.21 ka (UGA07OSL-500, Table 4) from near the top of the dunes at ACH1 section, Period 5 was also a time of dune reactivation during brief arid phases, particularly during the late Holocene (see also Tripaldi and Forman, 2007).

The sedimentary record from the SRP indicates that aggradation was governed mainly by ephemeral fluvial processes during two time intervals (Periods 1 and 3) from ca. 58–39 ka and ca. 36–24 ka. The climate at these times was semiarid and characterized by episodic flood events. In contrast, during the last glacial maximum, ca. 24–12 ka, the climate was windier and more arid and, as illustrated by the FA2 succession, aeolian transport and deposition dominated sedimentation north of the Diamante–Atuel fluvial system.

The inferred paleoenvironmental conditions from the SRP sections are in broad agreement with regional evidence. Prior to the last glacial maximum, fluvial reworking and hillslope processes were dominant at several Pampean localities (Kemp et al., 2004, 2006; Fucks and Deschamps, 2008). In the Andean piedmont of Tupungato, close to the Tunuyán city, 150 km northwest of the area examined here (Fig. 1c), alluvial aggradation was under way by ca. 50 ka BP (Toms et al., 2004). In that area, mollusc shells in fluvial deposits suggest relatively warm and wetter conditions from ca. 35.2 to 35.5 ^{14}C ka BP and ca. 31.5 to 31.6 ^{14}C ka BP (De Francesco et al., 2007). In the paleodune field of San Luis, 300 km northeast of SRP (Fig. 1b), a well-developed paleosol, formed on aeolian deposits with a basal OSL age of 32.7 ± 2.15 ka, records a period of landscape stability. The paleosol is truncated and buried by aeolian sand with OSL ages of 27.65 ± 2.08 ka and 25.09 ± 1.63 ka (Blowout section of Tripaldi and Forman, 2007). These records suggest an interstadial during the last glacial cycle. OSL ages for the SRP show that at ACH2 section this time period saw both fluvial and aeolian deposition accompanied by fluvial reworking of some aeolian deposits. It was also characterized by the development of oxidation features and root traces on top of FA1 at ACH1 section.

During the last glacial maximum, aeolian sedimentation documented by loess accumulation is evident at several Pampean localities (Kemp et al., 2006; Frechen et al., 2009; Zárate, et al., 2009). The earlier aeolian activity reported from the paleodune field of San Luis (Tripaldi and Forman, 2007) is likely the result of its different geomorphological setting in a distal plain far from the Andean piedmont and the San Luis ranges.

Aggradation across the SRP was punctuated by volcanic events such as the eruption that produced the pyroclastic deposits at ACH2 section. This volcanic event may have also deposited a tephra layer bracketed by OSL ages of 24.2 ± 1.1 and 22.3 ± 1.7 ka (Toms et al., 2004) in alluvial successions in the upper basin of the Tunuyán river (Fig. 1c). The occurrence of tephra layers is expected in the SRP, since it is situated in a still active volcanic district characterized by Quaternary volcanic activity (Ramos and Nullo, 1993). Very recent volcanism is documented by the Quizapú eruption in 1932 (Hildreth and Drake, 1992) recorded in the uppermost part of the SRP successions.

Conclusions

Late Quaternary aggradation of the SRP, in the distal Andean piedmont of Mendoza (34° 30′S), resulted from both fluvial and aeolian processes. OSL ages constrain these depositional events between ca. 58–13 ka. If uncertainties in the OSL ages are taken into account, the ages are in correct chronostratigraphic sequence suggesting that the record of past fluvial and aeolian events presented here is chronologically reliable.

From ca. 58 to 39 ka and from ca. 36 to 24 ka, during MIS 3 (59–24 ka; Martinson et al., 1987), fluvial deposition was dominant in ephemeral streams, mainly controlled by unconfined sheet flows and associated with fluvial–aeolian interaction (FA1), suggesting semiarid conditions at these times. After ca. 23 ka there was a major sedimentological change to a setting dominated by aeolian deposition (FA2) (at ACH 2 section two ages of ca. 23–20 ka and one of ca. 21–17 ka; at ACH 1 section one age of ca. 16–13 ka). Whether the aeolian deposits record one long dry windy interval extending from ca. 23–13 ka or two intervals from ca. 23–20 ka and ca. 16–13 ka is not yet clear and will require additional work to resolve. However, the data do indicate more arid and much windier conditions at the time of the last glacial maximum.

The oldest OSL ages of the aeolian sand from the upper part of the studied SRP deposits at the southern margin of the Médanos de los Naranjos dune field, suggest that dunes started to accumulate possibly as early as ca. 23 ka. This aeolian event was likely related to the arid and cold environmental conditions that prevailed in the Andean piedmont during the last glacial maximum.

Although more analyses are needed, it is reasonable to propose as a working hypothesis that the oxidation features and root traces on the top of the fluvial facies preceding deposition of the aeolian sand at the ACH1 section formed at the time of mild wetter and less windy interval in the SRP.

Acknowledgments

Financial support was provided by the CONICET-PIP5819 (to A. Tripaldi and M.A. Zárate), and by NSF grant 0725090 and the Franklin College of the University of Georgia (to G. Brook). We would like to thank G. Neme and A. Gil for logistical support during field work. Comments and suggestions from the Associate Editor ZhongPing Lai and two anonymous reviewers are highly appreciated and helped to improve the manuscript.

References

Abraham, E., Del Valle, H., Roig, F., Torres, L., Ares, J., Godagnone, R., 2009. Overview of the geography of the Monte Desert biome (Argentina). Journal of Arid Environment 73, 144–153.

Ahlbrandt, T.S., Fryberger, S., 1982. Introduction to eolian deposits. In: Scholle, P.A., Spearing, D. (Eds.), Sandstone Depositional Environments. American Association of Petroleum Geologists (AAPG), Tulsa, Memoir 31, pp. 11–47.

Aitken, M.J., 1985. Thermoluminescence Dating. Academic Press. 359 pp.

Aitken, M.J., 1998. An Introduction to Optical Dating: The Dating of Quaternary Sediments by the Use of Photon-stimulated Luminescence. Oxford University Press. 267 pp.

Blasi, A., Castiñeira Latorre, C., del Puerto, L., Prieto, A., Fucks, E., De Francesco, C., Hanson, P.R., García-Rodriguez, F., Huarte, R., Carbonari, J., Young, A., 2010. Paleoambientes de la cuenca media del río Luján (buenos Aires, Argentina) durante el último período glacial (EIO 2–4). Latin American journal of Sedimentology and Basin Análisis 17, 95–111.

Bøtter-Jensen, L., Duller, G.A.T., Murray, A.S., Banerjee, D., 1999. Blue light emitting diodes for optical stimulation of quartz in retrospective dosimetry and dating. Radiation Protection Dosimetry 84, 335–340.

Bridge, J.S., 2003. Rivers and Floodplains, Forms, Processes, and Sedimentary Record. Wiley-Blackwell. 504 pp.

Bull, W.B., 1997. Discontinuous ephemeral streams. Geomorphology 19, 227–276.

https://doi.org/10.1016/j.yqres.2011.06.008 Published online by Cambridge University Press

Bullard, J.E., Livingstone, I., 2002. Interactions between aeolian and fluvial systems in dryland environments. Area 34, 8–16.
Cabrera, A., 1971. Regiones Fitogeograficas Argentinas. Enciclopedia Argentina de Agricultura y Ganadería. ACME, Buenos Aires, Argentina, pp. 1–85. Tomo II, Fasc. I.
Cain, S.A., Mountney, N.P., 2009. Spatial and temporal evolution of a terminal fluvial fan system: the Permian Organ Rock Formation, South-east Utah, USA. Sedimentology 56, 1774–1800.
Cas, R.A.F., Wright, J.V., 1987. Volcanic Successions. Allen & Unwin, London. 528 pp.
Clapperton, C.M., 1993. Nature of environmental changes in South America at the Last Glacial Maximum. Palaeogeography, Palaeoclimatology, Palaeoecology 101, 189–208.
Colls, A.E., Stokes, S., Blum, M.D., Straffin, E., 2001. Age limits on the Late Quaternary evolution of the upper Loire River. Quaternary Science Reviews 20 (5–9), 743–750.
D'Antoni, H., 1983. Pollen analysis of Gruta del Indio. Quaternary South America and Antartica Peninssula 1, 83–104.
De Francesco, C.G., Zárate, M.A., Miquel, S.E., 2007. Late Pleistocene mollusc assemblages inferred from paleoenvironments from the Andean Piedmont of Mendoza, Argentina. Palaeogeography, Palaeoclimatology, Palaeoecology 257, 461–469.
Duller, G.A.T., 1999. Luminescence Analyst computer programme V2.18. Department of Geography and Environmental Sciences, University of Wales, Aberystwyth. 528 pp.
Espizúa, L.E., 2005. Holocene glacier chronology of Valenzuela Valley, Mendoza Andes, Argentina. The Holocene 15 (7), 1079–1085.
Folk, R.L., Ward, W.C., 1957. Brazos River bar — a study in the significance of grain-size parameters. Journal of Sedimentary Petrology 27 (1), 3–27.
Frechen, M., Seifert, B., Sanabria, J.A., Argüello, G.L., 2009. Chronology of late Pleistocene Pampa loess from the Córdoba area in Argentina. Journal of Quaternary Science 24, 761–772.
Fryberger, S.G., Ahlbrandt, T.S., Andrews, S.A., 1979. Origin, sedimentary features, and significance of low-angle eolian "sand sheet" deposits, Great Sand Dunes National Monument and Vicinity, Colorado. Journal of Sedimentary Petrology 49 (3), 733–746.
Fucks, E., Deschamps, C.M., 2008. Depósitos continentales cuaternarios en el noroeste de la provincia de Buenos Aires. Revista de la Asociación Geológica Argentina 63 (3), 326–343.
Glennie, K.W., 1970. Desert sedimentary environments. Developments in Sedimentology, 14. Elsevier. 222 pp.
González Díaz, E.F., 1972. Descripción geológica de la hoja 27d, San Rafael, provincia de Mendoza. Boletín 132. Ministerio de Industria y Minería — Servicio Nacional Minero Geológico, Buenos Aires, p. 144.
González Díaz, E.F., Fauqué, L., 1993. Geomorfología. In: Ramos, V. (Ed.), Geología y Recursos Naturales de Mendoza, XII Congreso Geológico Argentino y II Congreso de Exploración de Hidrocarburos. Relatorio, pp. 217–234.
Gosse, J., 1994. Relative dating of Quaternary deposits in the Rio Atuel Valley, Mendoza, Argentina, PhD thesis, Lehigh University Bethlehem, PA, 175 pp.
Guccione, M.J., 1993. Grain-size distribution of overbank sediment and its use to locate channel positions. In: Marzo, M., Puigdefábregas, C. (Eds.), Alluvial sedimentation: International Association of Sedimentologists Special Publication, 17, pp. 185–194.
Hampton, B.A., Horton, B.K., 2007. Sheetflow fluvial processes in a rapidly subsiding basin, Altiplano plateau, Bolivia. Sedimentology 54 (5), 1121–1148.
Hein, F.J., Walker, R.G., 1977. Bar evolution and development of stratification in the gravelly, braided Kicking Horse River, British Columbia. Canadian Journal Earth Science 14, 562–570.
Hildreth, W., Drake, R.E., 1992. Volcán Quizapu, Chilean Andes. Bulletin of Volcanology 54, 93–125.
Hunter, R.E., 1977a. Terminology of cross-stratified sedimentary layers and climbing-ripple structures. Journal of Sedimentary Petrology 47, 697–706.
Hunter, R.E., 1977b. Basic types of stratification in small eolian dunes. Sedimentology 24, 361–387.
Iriondo, M., 1999. Climatic changes in the South American plains: records of a continent-scale oscillation. Quaternary International 57 (58), 93–112.
Kemp, R.A., Toms, P.S., King, M., Kröhling, D.M., 2004. The pedosedimentary evolution and chronology of Tortugas, a Late Quaternary type-site of the northern Pampa, Argentina. Quaternary International 114 (1), 101–112.
Kemp, R.A., Zárate, M.A., Toms, P., King, M., Sanabria, J., Arguello, G., 2006. Late Quaternary paleosols, stratigraphy and landscape evolution in the Northern Pampa, Argentina. Quaternary Research 66 (1), 119–132.
Kocurek, G., Nielson, J., 1986. Conditions favourable for the formation of warm-climate aeolian sand sheets. Sedimentology 33, 795–816.
Krömer, R., 1996. Los sedimentos cuaternarios del sudeste de la llanura mendocina. Implicancias paleoclimáticas. Multequina 5, 49–55.
Langford, R.P., 1989. Fluvial-aeolian interactions: part I, modern systems. Sedimentology 36, 1023–1035.
Markey, B.G., Bøtter-Jensen, L., Duller, G.A.T., 1997. A new flexible system for measuring thermally and optically stimulated luminescence. Radiation Measurements 27, 83–90.
Markgraf, V., 1983. Late and postglacial vegetational and paleoclimatic changes in subantarctic, temperate and arid environments in Argentina. Palynology 7, 43–70.
Martinson, D.G., Pisias, N.G., Hays, J.D., Imbrie, J., Moore Jr., T.C., Shackleton, N.J., 1987. Age dating and the orbital theory of the ice ages: development of a high-resolution 0 to 300,000-year chronostratigraphy. Quaternary Research 27, 1–29.
McKee, E.D., Crosby, E.J., Be, H.L., 1967. Flood Deposits, Bijou Creek, Colorado. Journal of Sedimentary Research 37 (3), 829–851.
Miall, A.D., 1977. A review of the braided river depositional environment. Earth Science Review 13, 1–62.
Miall, A.D., 1996. The Geology of Fluvial Deposits. Springer Verlag, Berlín.
Murray, A.S., Wintle, A.G., 2000. Luminescence dating of quartz using improved single-aliquot regenerative-dose protocol. Radiation Measurement 32, 57–73.
Nanson, G.C., Croke, J.C., 1992. A genetic classification of floodplains. Geomorphology 4, 459–486.
Newell, A.J., 2001. Bounding surfaces in mixed aeolian-fluvial system (Rotliegend, Wessex Basin, SW UK). Marine and Petroleum Geology 18, 339–347.
Perelló, M.J., Tripaldi, A., Zárate, M., 2009. Sedimentología y geomorfología de los Médanos de la Travesía (sur de Mendoza, Argentina). IV Congreso Argentino de Cuaternario y Geomorfología, XII Congresso da Associação Brasileira de Estudos do Quaternário y II Reunión sobre el Cuaternario de América del Sur: Actas, 274. La Plata. Asociación Argentina de Cuaternario y Geomorfología.
Polanski, J., 1963. Estratigrafía, neotectónica y geomorfología del Pleistoceno pedemontano, entre los ríos Diamante y Mendoza. Revista de la Asociación Geológica Argentina 37 (3–4), 127–349.
Prescott, J.R., Hutton, J.T., 1994. Cosmic ray contributions to dose rates for luminescence and ESR dating: large depths and long-term time variations. Radiation Measurements 23, 497–500.
Prieto, A.R., Blasi, A.M., De Francesco, C.G., Fernández, C., 2004. Environmental history since 11,000 yr B.P. of the northeastern Pampas, Argentina from alluvial sequences of Luján River. Quaternary Research 62, 146–161.
Prohaska, F., 1976. The climate of Argentina, Paraguay and Uruguay. In: Schwerdtfeger, W. (Ed.), Climates of Central and South America. World Survey of Climatology. Elsevier, Amsterdam, pp. 13–73.
Pye, K., Tsoar, H., 1990. Aeolian Sand and Sand Dunes. Unwin Hyman, London. 458 pp.
Ramos, V.A., Kay, S.M., 2006. Overview of the tectonic evolution of the southern central Andes of Mendoza and Neuquén (35°–39° S latitude). In: Ramos, V.A., Kay, S.M. (Eds.), Evolution of an Andean margin: a tectonic and magmatic view from the Andes to the Neuquén Basin (35°–39° S lat): The Geological Society of America, Special Paper, 407, pp. 1–18.
Ramos, V., Nullo, F., 1993. El volcanismo de arco cenozoico. In: Ramos, V.A. (Ed.), Geología y Recursos Naturales de Mendoza, XII Congreso Geológico Argentino y II Congreso de Exploración de Hidrocarburos. Relatorio, Mendoza, pp. 149–160.
Rodríguez, E., Barton, M., 1993. El Cuaternario de la llanura. In: Ramos, V. (Ed.), Geología y Recursos Naturales de Mendoza, XII Congreso Geológico Argentino y II Congreso de Exploración de Hidrocarburos. Relatorio, Mendoza, pp. 173–194.
Rundel, P.W., Villagra, P.E., Dillon, M.O., Roig-Juñent, S., Debandi, G., 2007. Arid and semi-arid ecosystems. In: Veblen, T.K., Young, K.R., Orme, A. (Eds.), The Physical Geography of South America. Oxford University Press, Oxford, pp. 158–183.
Sepúlveda, E., Carpio, F., Regairaz, M., Zanettini, J., Zárate, M.A., 2007. Hoja Geológica 3569-II, San Rafael, provincia de Mendoza. Instituto de Geología y Recursos Minerales, Servicio Geológico Minero Argentino. Boletín 321. Segunda edición revisada, 59 pp. Buenos Aires.
Stokes, S., Bray, H.E., Blum, M.D., 2001. Optical resetting in large drainage basins: tests of zeroing assumptions using singlealiquot procedures. Quaternary Science Reviews 20, 879–886.
Svendsen, J., Stollhofen, H., Krapf, C.B.E., Stanistreet, I.G., 2003. Mass and hyperconcentrated flow deposits record dune damming and catastrophic breakthrough of ephemeral rivers, Skeleton Coast Erg, Namibia. Sedimentary Geology 160, 7–31.
Teruggi, M.E., 1957. The nature and origin of Argentine loess. Journal of Sedimentary Petrology 27, 322–332.
Toms, P.S., King, M., Zárate, M.A., Kemp, R.A., Foit, F.F., 2004. Geochemical characterization, correlation and optical dating of tephra in alluvial sequences of central western Argentina. Quaternary Research 62, 60–75.
Tonni, E.P., Nabel, P., Cione, A.L., Etchichury, M., Tófalo, R., Scillato Yané, G., San Cristóbal, J., Carlini, A., Vargas, D., 1999. The Ensenada and Buenos Aires formations (Pleistocene) in a quarry near La Plata, Argentina. Journal of South American Earth Sciences 12, 273–291.
Tripaldi, A., 2010. Campos de dunas de la planicie sanrafaelina: patrones de dunas e inferencias paleoclimáticas para el Pleistoceno tardío-Holoceno. In: Zárate, M.A., Gil, A., Neme, G. (Eds.), Paleoambientes y ocupaciones humanas del centro-oeste de Argentina durante la transición Pleistoceno–Holoceno y Holoceno. Sociedad Argentina de Antropología, Buenos Aires, pp. 65–93.
Tripaldi, A., Forman, S.L., 2007. Geomorphology and chronology of Late Quaternary dune fields of western Argentina. Palaeogeography, Palaeoclimatology, Palaeoecology 251, 300–320.
Tripaldi, A., Limarino, C.O., 2008. Ambientes de interacción eólica-fluvial en valles intermontanos: ejemplos actuales y antiguos. Latin American Journal of Sedimentology and Basin Analysis 15 (1), 43–66.
Tripaldi, A., Zárate, M.A., Brook, G.A., 2010. Sucesiones eólicas y fluviales del Pleistoceno tardío–Holoceno de la planicie sanrafaelina. In: Zárate, M.A., Gil, A., Neme, G. (Eds.), Paleoambientes y ocupaciones humanas del centro–oeste de Argentina durante la transición Pleistoceno–Holoceno y Holoceno. Sociedad Argentina de Antropología, Buenos Aires, pp. 95–121.
Wallinga, J., 2001. On the detection of OSL age overestimation using single-aliquot techniques. Geochronometria 21, 17–26.
Williams, G.E., 1971. Flood deposits of the sand-bed ephemeral streams of central Australia. Sedimentology 17, 1–40.
Zárate, M., 2003. Loess of southern South America. Quaternary Science Reviews 22, 1987–2006.
Zárate, M., Kemp, R., Toms, P., 2009. Late Quaternary landscape reconstruction and geochronology in the northern Pampas of Buenos Aires province, Argentina. Journal of South American Earth Sciences 27, 88–99.
Zhang, J.F., Zhou, L.P., Yue, S.Y., 2003. Dating fluvial sediments by optically stimulated luminescence: selection of equivalent doses for age calculation. Quaternary Science Reviews 22, 1123–1129.